NANO LETTERS

Letter

pubs.acs.org/NanoLett

PbSe Quantum Dot Field-Effect Transistors with Air-Stable Electron Mobilities above 7 cm^2 V^{-1} s^{-1}

Yao Liu,[†,⊥] Jason Tolentino,[†,‡,⊥] Markelle Gibbs,[†] Rachelle Ihly,[†] Craig L. Perkins,[§] Yu Liu,[∥] Nathan Crawford,[†] John C. Hemminger,[†] and Matt Law*[,†,‡]

[†]Department of Chemistry and [‡]Department of Chemical Engineering and Materials Science, University of California, Irvine, Irvine, California 92697, United States

[§]National Renewable Energy Laboratory, Golden, Colorado 80401, United States

[∥]Department of Physics and Astronomy, University of California, Irvine, Irvine, California 92697, United States

Supporting Information

ABSTRACT: PbSe quantum dot (QD) field effect transistors (FETs) with air-stable electron mobilities above 7 cm^2 V^{-1} s^{-1} are made by infilling sulfide-capped QD films with amorphous alumina using low-temperature atomic layer deposition (ALD). This high mobility is achieved by combining strong electronic coupling (from the ultrasmall sulfide ligands) with passivation of surface states by the ALD coating. A series of control experiments rule out alternative explanations. Partial infilling tunes the electrical characteristics of the FETs.

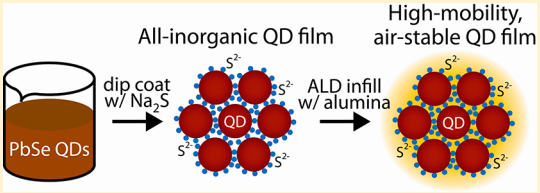

KEYWORDS: *Quantum dots, nanocrystals, lead selenide, field-effect transistors, solar cells*

The recent introduction of metal chalcogenide complexes (MCCs) as ligands for colloidal quantum dots (QDs)[1] has triggered a flurry of research into inorganic ligands for fabricating high-performance all-inorganic QD solids for optoelectronic applications.[2−4] In addition to several demonstrations of MCC efficacy by Talapin and co-workers,[5−8] a variety of metal-free inorganic ions including chalcogenides,[9,10] halides,[11] thiocyanate,[12−14] and trialkyl oxonium[15] have been shown in initial studies to provide generally better performance in CdX and PbX (X = S, Se, Te) QD field-effect transistors (FETs)[6,7,12−14] and solar cells[11] than the small molecules, such as hydrazine[16] and 1,2-ethanedithiol (EDT),[17,18] traditionally used to replace the long-chain insulating organic ligands inherited from QD synthesis. Ionic inorganic ligands offer several key advantages over neutral molecular ligands. First, many inorganic ligands are ultrasmall and enable strong electronic coupling between QDs in films, which favors high-mobility transport. Second, inorganic ions can quantitatively replace native long-chain ligands on the QD surface to produce charge-stabilized colloidal QD suspensions in polar media, in principle allowing the direct formation of conductive QD films from solution without the need for postassembly chemical or thermal treatments that can inhibit charge transport by increasing spatial and energetic disorder in the films. In practice, however, thermal treatments (150−300 °C) are typically needed to achieve good transport in all-inorganic QD solids. Also, solution-phase exchange has so far failed to yield stable all-inorganic PbX QD colloids except with select hydrazine-free MCCs or mixed chalcogenide ions,[5,13] so postassembly ("solid state") ligand exchange has been employed instead to make PbX QD devices.[10−13,15] A third advantage of inorganic ligands is that they decompose, evaporate, or assimilate into the QDs at relatively low temperatures to create functional inorganic matrices (e.g., with MCCs) or direct QD−QD contact and partial QD necking/fusion (e.g., with S^{2-} and SCN^-). Despite the large site energy disorder induced by such annealing,[7,14,19] the electronic properties of films made with this approach may be adequate for many applications, including high-efficiency solar energy conversion. Recent reports of record mobilities for electrons in CdSe,[7,14] holes in PbX,[12,15] and electrons in PbSe[20] QD films (~30, 3−4, and 5−10 cm^2 V^{-1} s^{-1}, respectively) may also reflect the onset of extended state or even bandlike transport (however, see ref 19), and together illustrate the promise of all-inorganic QD solids as a technology platform for high-performance, low-cost, large-area optoelectronics.

The use of ultrasmall inorganic ligands is not enough to guarantee high carrier mobility and good transport in QD films, even in the limit of perfect QD monodispersity. This is because surface states within the QD band gap (donors, acceptors, traps, recombination centers) can dominate transport and offset the advantage of strong electronic coupling from compact ligands, direct interdot contact, and QD necking. A QD device must be designed to eliminate or accommodate the largest source of energy disorder—the density of states within the band gap—in order to realize the full benefits of strong coupling. A variety of recent studies provide evidence for the existence of deep gap states[11,21,22] and Urbach tails[23,24] in PbX

Received: December 25, 2012
Revised: February 17, 2013
Published: March 1, 2013

   dx.doi.org/10.1021/nl304753n | *Nano Lett.* 2013, 13, 1578−1587

QD films. Recent reports of high-mobility QD FETs illustrate the importance of dealing with gap states. For example, Choi et al. found that trap filling by indium diffusion doping at 250 °C was required to improve the electron mobility of thiocyanate-capped CdSe QD FETs from <0.01 to 27 $cm^2\ V^{-1}\ s^{-1}$.[14] Also, Chung et al. achieved high mobilities in annealed $In_2Se_4^{2-}$ capped CdSe QD FETs in part by using a high-capacitance gate dielectric to accumulate a large carrier density that fills traps in the QD films.[7] Mobility in QD and other disordered semiconductor FETs usually increases with larger gate-induced carrier densities,[25,26] which serves as an important reminder that field-effect mobility is a "filled trap" mobility that depends on device geometry and biasing conditions and is not an intrinsic property of a QD film. These successful approaches to trap filling and doping in CdSe QD FETs may not be as useful for two-terminal devices (e.g., solar cells) or less stable QD materials (e.g., PbX) that tend to sinter above ∼150 °C.[27] Alternative approaches to passivating traps and controlling doping in highly-coupled QD films would aid in the rational fabrication of high-performance QD solar cells.

Recently, low-temperature atomic layer deposition (ALD) has been used to gently infill the pore space of conductive PbX QD films with conformal metal oxides to produce nanocomposites with vastly improved oxidative and photothermal stability and enhanced performance in FETs and solar cells.[27,28] The aim of the ALD coating is to serve as a gas diffusion barrier to stop oxidation, a nanoscale cement to inhibit solid-state diffusion within the films, and an electronic matrix that passivates surface states and reduces the size of the inter-QD tunnel barrier governing charge transport in QD films. Similar aims motivate the use of MCCs[1] and other strategies[29] to engineer the interdot matrix. ALD employs alternating self-saturating surface reactions of gas-phase precursors to deposit conformal thin films of precisely controlled thickness.[30] ALD infilling of QD films leverages the unrivaled ability of ALD to uniformly coat high aspect ratio structures, including the networks of narrow channels and pockets of nanoporous materials, without premature clogging near the sample surface. Many different materials, including oxides, chalcogenides, nitrides, and metals,[31] can be deposited by ALD at sufficiently low temperatures (<80 °C) to avoid ripening and sintering of even the most thermally-unstable QDs, and ALD infilling is effective even with quite small QDs (∼3 nm).[28] Several materials can be deposited in sequence to make functional multicomponent ALD infills.[28] Furthermore, since annealing is not needed to activate transport, ALD infilling is expected to induce much less site energy disorder than methods requiring ligand decomposition above 200 °C. ALD is thus a promising way to make a variety of functional and environmentally robust QD-based thin film materials.

In this paper, we demonstrate electron mobilities above 7 $cm^2\ V^{-1}\ s^{-1}$ in ambipolar PbSe QD FETs by using ALD infilling of amorphous alumina (a-Al_2O_3) to reduce the density of surface states and tune the carrier concentration in QD films prepared via dip coating with sodium sulfide (Na_2S) ligand exchange. Sulfide capping results in a very small interdot distance, strong electronic coupling, and high-conductance p-channel FETs prior to infilling. Alumina infilling is found to systematically lower the free hole concentration by eliminating acceptors at the QD surface. As a result, the FETs evolve from p-channel to ambipolar and then to dominant n-channel behavior with linear electron mobilities of 4−5 $cm^2\ V^{-1}\ s^{-1}$ and 6−8 $cm^2\ V^{-1}\ s^{-1}$ for fully infilled devices made at ALD temperatures of 54 and 75 °C, respectively. The increase in mobility with both ALD temperature and the number of ALD cycles shows that infilling passivates electron traps as well as acceptors. Using partial ALD infilling, we can control the dominant carrier type and equilibrium film conductivity to make p-type films that feature high minority carrier mobilities, favorable for efficient thin-film QD solar cells. These mobility values are equal to the highest yet reported for PbX QD FETs. Moreover, the ALD coating renders the FETs indefinitely stable in air. These sulfide-treated, ALD-infilled PbSe QD FETs are the first high-mobility, air-stable PbX QD solids and should be useful in the development of high-performance QD optoelectronic devices.

Methods. *Chemicals.* Lead oxide (PbO, 99.999%), selenium (99.99%), oleic acid (OA, tech. grade, 90%), diphenylphosphine (DPP, 98%), trioctylphosphine (TOP, tech. grade, >90%), 1-octadecene (ODE, 90%), 1,2-ethanedithiol (EDT, >98%), trimethylaluminum (97%), and anhydrous solvents were purchased from Aldrich and used as received. Anhydrous sodium sulfide was acquired from Strem and stored in a glovebox.

QD Synthesis. PbSe QDs were synthesized and purified using standard airfree techniques. In a typical synthesis, a solution of 1.09 g PbO (4.9 mmol), 3.45 g oleic acid (12.2 mmol), and 13.5 g ODE was degassed in a three-neck flask and heated at 180 °C for one hour to dissolve the PbO and dry the solution. Fifteen milliliters of a 1 M solution of TOP-Se containing 0.14 g of DPP (0.75 mmol) was then rapidly injected into this hot solution. The QDs were grown for short times (1−4 min), and the reaction was then quenched with a water bath and 20 mL of anhydrous hexane. The QDs were purified by three rounds of dispersion/precipitation in hexane/ethanol and stored in a glovebox as a powder.

QD Film Deposition. A mechanical dip coater mounted inside of a glovebox (DC Multi-4, Nima Technology) was used to prepare PbSe QD films via a layer-by-layer procedure described in detail elsewhere.[32] Briefly, the substrates (glass, silicon, quartz, or prepatterned FET or sapphire substrates, cleaned by sonication in acetone followed by rinses in acetone and isopropanol and dried under N_2 flow) were alternately dipped into a 2 mg mL^{-1} solution of QDs in dry hexane and then a 0.5 mM solution of sodium sulfide in dry methanol. A third beaker containing neat dry methanol was used to rinse the films after each dip in the sulfide solution in order to remove any residual ions. We fabricated films with thicknesses in the range of 25−350 nm (thin for FETs, thicker for XPS, UV−vis, FTIR, SIMS, and XRD studies). Films of oleate-capped QDs ("as made films") were made by spin coating a 100 mg mL^{-1} solution of QDs in octane at 600 rpm for 30 s, followed by 1200 rpm for 30 s.

Atomic Layer Deposition Infilling. Amorphous Al_2O_3 was deposited in a homemade cold-wall traveling wave ALD system within a glovebox from trimethylaluminum and water at a substrate temperature of 27−125 °C and an operating pressure of ∼0.1 Torr. Pulse and purge times were 20 ms and 90−120 s, respectively. Synthesis of a 25 nm ALD film requires ∼9 h with these parameters, varying somewhat with temperature. ALD film thicknesses were determined via scanning electron microscopy (SEM) and ellipsometry on planar silicon substrates.

Characterization. Transmission electron microscopy (TEM) characterization was performed on a Philips CM20 operating at 200 kV. SEM images were acquired on an FEI

dx.doi.org/10.1021/nl304753n | Nano Lett. 2013, 13, 1578−1587

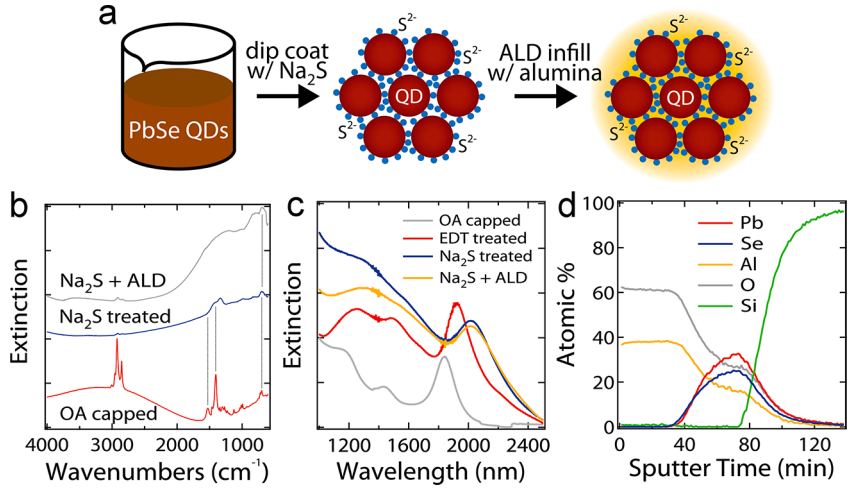

Figure 1. Basic characterization of sulfide-exchanged, alumina-infilled, 6.3 nm diameter PbSe QD thin films. (a) Cartoon of the fabrication process. Layer-by-layer dip coating with sodium sulfide ligand exchange yields sulfide-capped films, which are then infilled with ALD alumina (yellow matrix). (b) FTIR spectra of an oleate-capped QD film (made by spin coating) and sulfide-capped QD films before and after ALD infilling (all on silicon substrates). The spectra have been scaled to normalize the film thickness. The integrated C−H stretch intensity decreases by >97.5% after sulfide ligand exchange. Dotted lines are guides to the eye. (c) Comparative optical extinction spectra of oleate-capped (gray), EDT-exchanged (red), sulfide-exchanged (blue), and sulfide-exchanged and ALD-infilled QD films (orange) on glass substrates. The spectra are aligned at 2500 nm. Note that the weak scattering tail extending past 2500 nm is not shown. Film thicknesses: ∼150 nm. See Figure S1 in the Supporting Information for similar spectra of 5.1 nm diameter QDs. (d) XPS depth profile of a ∼150 nm thick sulfide-treated, alumina-infilled QD film on a silicon substrate. Alumina thickness for all samples: ∼25 nm. ALD temperature: 54 °C.

Magellan 400 instrument. Optical absorption spectra were acquired with a PerkinElmer Lambda 950 spectrophotometer operating in transmission mode. Samples were sealed within cells consisting of two mated 1.33″ ConFlat sapphire viewports. Films mounted in these cells show negligible oxidation after months of storage in air. FTIR measurements were carried out on nanocrystal films deposited on double side polished intrinsic silicon substrates using a JASCO 4100 FTIR spectrometer. X-ray diffraction patterns of the QD films were collected with a Rigaku Ultima III diffractometer with Cu Kα irradiation.

XPS depth profiles were acquired using a modified Physical Electronics 5600 XPS with monochromatic Al Kα radiation (1486.6 eV) and a pass energy of 29 eV. The films were found to charge slightly during analysis, so spectra were aligned by placing the Pb $4f_{7/2}$ peak at the lowest observed binding energy of 137.3 eV. Additional XPS measurements were performed with an ESCALAB MKII surface analysis instrument (VG Scientific) using Al Kα X-rays in constant energy mode with pass energies of 100 and 20 eV for survey scans and narrow scans, respectively. Binding energies were charge corrected by using Au foil to calibrate with respect to the Au 4f peak at 84.0 eV.

Secondary ion mass spectrometry (SIMS) was performed by Evans Analytical Group on a Cameca dynamic SIMS instrument using 14.5 keV Cs ions for anions (C, S, P, Si) and 8 keV O_2 ions for cations (Na, Pb, Al, Zn, Ca, Fe, Ti). All elements were quantified based on a Si standard. Estimated detection limits were (in atoms/cm^3) 1×10^{14} for Na and Ti, 1×10^{15} for Ca, 3×10^{15} for P, 1×10^{16} for Zn and Fe, 4×10^{16} for S, and 5×10^{17} for C. Atomic concentrations are accurate to within a factor of 5. The depth scale was quantified by measuring the analysis craters with a stylus profilometer and confirmed by SEM imaging of the sectioned films.

DFT Modeling. Estimates of the interdot distance were calculated using density functional theory (DFT). Two PbSe slabs separated with either S^{2-} or EDT^{2-} ligands were modeled at the PBE/def2-SVP level[33,34] using the RI-J method in the TURBOMOLE 6.4 software package.[35] Two triangular slabs of $[Pb_{64}Se_{59}]^{10+}$ were aligned with their Pb {111} surfaces facing each other. Ten S^{2-} or EDT^{2-} ligands were inserted between the slabs, and the neutral system was allowed to relax to an energy minimum (total energy converged to 10^{-6} Hartree and the Cartesian gradient norm to 10^{-3} atomic units).

The slabs were not constrained to be parallel and flat over their entire area, but the core of each system remained relatively parallel through the minimization procedure. Estimates of the interslab distance were derived from the hexagonal core of seven Pb ions on each surface. The core was oriented to minimize the scatter of Cartesian z-coordinate values within each "plane". Interplane distances were then taken as the difference between the average z-values of each plane, and error estimates from the sum of the standard deviations of the z-values within each plane.

Field-Effect Transistor Measurements. QD films were dip coated onto degenerately doped silicon substrates coated with a 200 nm thick thermal SiO_2 gate oxide and prepatterned with source/drain electrodes (5 nm Ti/35 nm Au, 25 μm channel length, 1000 μm width unless otherwise noted). QD film thicknesses of 20−35 nm (4−7 QDs thick) were used. The perimeter of each QD film was wiped clean with a cleanroom swab to eliminate parasitic gate currents and provide a clean spot for contacting the gate electrode. FET measurements at room temperature were performed in an N_2-filled glovebox with a homemade probe station using a Keithley 2636A dual-channel SourceMeter and a Keithley 238 SMU (for gated 4-point FET studies) driven by LabVIEW software. Low-temperature FET measurements used a Janis ST-100 cryostat outfitted with a custom 5-probe sample mount. Liquid nitrogen was used to vary the sample temperature between 80 and 300 K in a dynamic vacuum of 10^{-7} Torr. Linear mobilities, μ_{lin}, were calculated from transfer curves acquired at $V_{SD} = \pm 10$ V (with

dx.doi.org/10.1021/nl304753n | Nano Lett. 2013, 13, 1578−1587

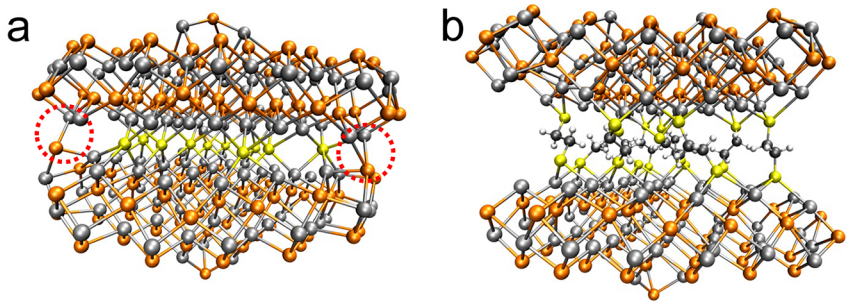

Figure 2. DFT structural models of ligand-bridged Pb-terminated PbSe {111} slabs. (a) Sulfide ligands. The interdot distance is 3.76 ± 0.06 Å. Dashed circles indicate regions of interdot necking apparent in the simulation. (b) EDT ligands. The interdot distance is 6.4 ± 0.19 Å. Gray spheres = Pb, orange = Se, yellow = S, black = C, white = H.

positive V_{SD} for electrons and negative V_{SD} for holes), according to the gradual channel approximation equation in the linear regime:

$$\left.\frac{dI_D}{dV_G}\right|_{V_{SD}=\text{constant}} = \frac{WC_{ox}V_{SD}}{L}\mu_{lin}(V_G, V_{SD}) \quad (1)$$

where the channel width is W, the channel length is L, and the capacitance of the gate oxide per unit area is C_{ox} (17.5 nF cm^{-2}). This expression acknowledges that the mobility in disordered systems may be a function of V_G and V_{SD}, as discussed in the text. Except where noted, the slope of the transfer curves for linear mobility calculations was measured at V_G = ±40 V, such that $|V_G - V_T| > 3|V_{SD}|$, where V_T is the threshold voltage, to ensure only one type of carrier (either electrons or holes) dominated the current. V_G = ±40 V corresponds to an average induced charge carrier concentration of $n_{ind} = C_{ox}(V_G - V_D/2 - V_T)/e \approx 3.5 \times 10^{12}$ charges/cm^2 for fully infilled FETs (where $|V_T| < 5$ V), which equates to ~1.6 and ~1.1 charges per QD for 6.3 and 5.1 nm QDs, respectively, assuming that the charges are located only in the first monolayer of QDs (see the discussion of the accumulation layer thickness in the Supporting Information). This assumption may overestimate the induced charge density by as much as a factor of 3. V_{SD} and V_G sweep rates were 50 V/s unless otherwise noted. Mobility data were reproduced at least three times using nominally identical samples.

Qualitative thermopower measurements were carried out in a glovebox using a cold plate to establish an ~80 K temperature gradient across the samples and a Keithley 2636 SourceMeter to determine the majority carrier type.

Results and Discussion. PbSe QD films were prepared by layer-by-layer dip coating[17] using sodium sulfide ligand exchange (0.5 mM Na_2S in anhydrous MeOH) followed by ALD infilling with amorphous alumina[28] (see Methods). A cartoon of the fabrication process is shown in Figure 1a. FTIR extinction spectra (4000−600 cm^{-1}) of sulfide-exchanged, 6.3 nm diameter QD films before and after ALD infilling were compared with spectra of oleate-capped QD films (prepared by spin coating) to quantify the extent of oleate ligand removal (Figure 1b). Sulfide exchange results in >97.5% reduction of the integrated C−H stretch signal, consistent with quantitative removal of oleate by sulfide, as expected from an earlier report of solution-phase sulfide ligand exchange of CdX and PbS QDs.[36] Alumina infilling of sulfide-exchanged films causes insignificant additional changes to the C−H signal. Figure 1c compares UV−vis−IR extinction spectra of these films (on glass substrates), along with a typical film prepared by dip coating using 1,2-ethanedithiol (EDT), a common organic ligand for making conductive PbX QD solids.[2,17] The first exciton absorption peak shifts from 1840 nm (0.674 eV) for the oleate-capped films to 1933 nm (0.642 eV) for EDT-treated films, 2020 nm for sulfide-treated films, and 2020 nm (0.614 eV) for sulfide-treated and ALD infilled films (redshifts of 32, 60, and 60 meV, respectively). The corresponding excitonic peak widths are 62, 59, 80, and 88 meV. Thus, exchange with sulfide rather than EDT results in a factor of 2 larger redshift as well as substantial peak broadening. We attribute this large redshift/broadening to the very small interdot distance in the sulfide-exchanged films resulting in (i) enhanced dielectric screening, (ii) especially strong electronic coupling, and (iii) partial QD necking, all of which can decrease the average confinement energy (redshift) and increase the spread in confinement energies (broadening). Indeed, DFT models of idealized Pb-terminated PbSe {111} slabs bridged by a ligand monolayer show an interdot distance (defined as the average distance between surface Pb atoms perpendicular to the slabs) of 3.76 ± 0.06 Å with sulfide ligands versus 6.4 ± 0.19 Å with EDT ligands (Figure 2). The very small interdot distance with sulfide capping is expected to facilitate direct Pb−Se bonding between the QDs (i.e., necking and fusion) at low temperatures. Interestingly, our simulations clearly show the tendency of sulfide-capped QDs to neck (dashed circles in Figure 2). We believe that necking is common in QD films capped by ultrasmall inorganic ligands and may explain much of the redshifting and broadening observed in recent studies.[7,10,14,19] We note that ALD infilling of sulfide-exchanged films causes no additional peak shift but some additional broadening, suggesting that deposition of the alumina matrix further increases dielectric screening, electronic coupling, and QD necking, although the relative importance of these different factors is not clear at this time.

We used X-ray photoelectron spectroscopy (XPS) and secondary ion mass spectrometry (SIMS) depth profiling to characterize the layer structure and elemental composition of the infilled QD films. A typical XPS profile of a ~150 nm thick QD film coated with ~25 nm of ALD alumina at 54 °C (Figure 1d) shows that alumina indeed infills the interstitial spaces within the QD film, as we recently reported for films treated with EDT and other organic ligands.[28] The sample therefore consists of a layer of pure Al_2O_3 on top of a PbSe/Al_2O_3 nanocomposite film. Sulfur was detected by XPS in the PbSe/Al_2O_3 layer, but the sulfur concentration could not be accurately quantified due to interference from selenium in S 2s and 2p spectra. Sodium, meanwhile, was below the XPS

dx.doi.org/10.1021/nl304753n | Nano Lett. 2013, 13, 1578−1587

detection limit (~0.1 atom %), while carbon was detected only at the film surface and is therefore not plotted in Figure 1d.

Figure 3 shows SIMS depth profiles for a ~270 nm thick QD film coated with ~25 nm of ALD alumina at 54 °C on an intrinsic (undoped) silicon substrate. Profiles of the matrix elements Pb, Al, and Si (top panel of Figure 3) confirm that alumina infills and overcoats the QD film, which is in agreement with the XPS data in Figure 1d. We measured the concentrations of S, Na, C, P, Zn, Ca, Ti, and Fe as a function of depth in the film (bottom panel of Figure 3). These elements were selected for analysis because they are used in the QD synthesis (C, P) or ligand exchange (S, Na) or because they are suspected impurities in the PbO starting material (Zn, Ca, Ti, Fe). We find that sulfur is present at a concentration of 1×10^{21} atoms/cm^3 in the QD layer (~1.5 atom %), which is nearly equal to the calculated concentration of Pb surface atoms in a random close-packed film of 6.3 nm PbSe QDs ($\sim 3 \times 10^{21}$ atoms/cm^3). We conclude that sulfur exists as approximately a monolayer on the QD surfaces and that the QDs are indeed sulfide capped. The concentration of sodium, however, is 10^4 times smaller than that of sulfur (1×10^{17} atoms/cm^3, or ~1.5 ppm), meaning that there is essentially no sodium in the films. We find only 0.1–0.5 atom % carbon in the QD composite layer, which is consistent with quantitative oleate removal by sulfide (Figure 1b). The carbon residue is probably an unavoidable legacy of the wet chemistry and trimethylaluminum ALD precursor used to make these films. Phosphorus is present at 20–90 ppm in the QD layer (presumably from TOP and DPP employed in the QD synthesis). There is a small amount of zinc (~10 ppm) in the alumina overlayer, which falls to less than 200 ppb in the QD layer. Ca and Ti were detected in trace quantities in the QD layer (650 and 40 ppb, respectively), while everywhere the iron concentration was lower than its detection limit (<100 ppb, not plotted). In summary, the SIMS and XPS data are in excellent agreement and together show that these films consist of infilled and overcoated sulfide-capped QDs containing <0.5 atom % carbon, < 100 ppm phosphorus, and only trace sodium, zinc, and other expected cations.

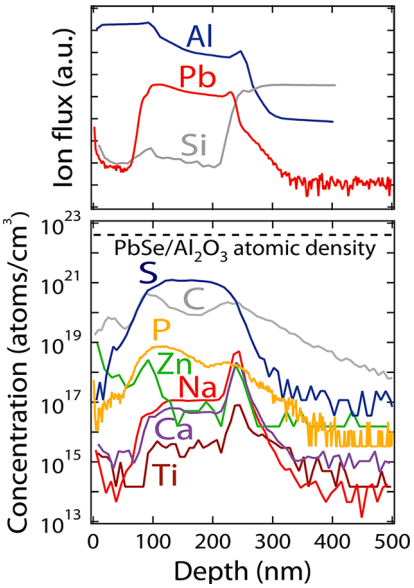

Figure 3. SIMS depth profiles of a ~270 nm thick sulfide-treated, ALD-infilled QD film on a silicon substrate. The top panel shows matrix elements and the bottom panel shows impurity elements. The concentrations of all impurity elements fall below their detection limits upon sputtering into the silicon substrate. The atomic density of the $PbSe/Al_2O_3$ layer is calculated for a 50:50 mixture of PbSe and amorphous alumina with a 20% void fraction. QD diameter: 6.3 nm. Alumina thickness: ~25 nm. ALD temperature: 54 °C. See Methods for SIMS experimental details.

We note that the absence of alkali cations in the films suggests that charge neutrality is maintained solely by anion exchange during dip coating. An idealized ligand exchange reaction for a single 6.3 nm QD that is consistent with our FTIR, SIMS, and elemental analysis data as well as the recent report by Zhang et al. on sulfide-exchanged PbS QDs[10] may be written as

$$(Pb_{1.165}Se)_{2110}(oleate)_{696} + 348\ Na_2S \rightarrow (Pb_{1.165}Se)_{2110}S_{348} + 696\ Na(oleate)$$

with the sodium oleate sequestering into the methanol rather than absorbing in the film. Here we assume a spherical QD with a stoichiometric core and excess Pb ions at the surface, two oleate ligands per excess Pb^{2+} (~6 oleate/nm^2),[37,38] and 100% ligand exchange. The QD stoichiometry ($Pb_{1.165}Se$) is based on our ICP-OES analysis of 6.0 nm PbSe QDs and is similar to previous reports.[38,39]

QD thin film FETs were fabricated by dip coating QD films onto prepatterned Ti/Au source/drain electrodes on Si/SiO_2 substrates (200 nm SiO_2). Figure 4 shows output curves (I_D–V_{SD}) and transfer curves (I_D–V_G) of a typical sulfide-capped, 6.3 nm PbSe QD FET before and after deposition of 18 nm of alumina by ALD at 54 °C (in all experiments, the first several nanometers of ALD alumina infills and the rest overcoats the QD film). Before ALD, the device shows high p-channel

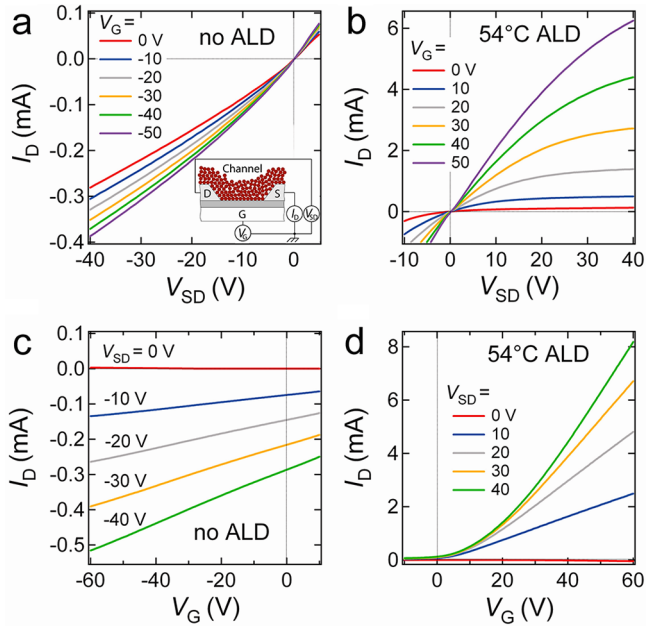

Figure 4. I–V plots of sulfide-capped PbSe QD FETs before and after ALD infilling at 54 °C. (a,b) Output plots. Inset is a schematic of the device. (c,d) Transfer plots. All data were acquired at room temperature. QD diameter = 6.3 nm; QD film thickness = 20–35 nm; alumina thickness = 18 nm; Channel dimensions: length = 25 μm; width = 1000 μm. Sweep rates = 50 V/s. Similar data for a FET infilled at 75 °C can be found in Supporting Information Figure S2.

dx.doi.org/10.1021/nl304753n | Nano Lett. 2013, 13, 1578–1587

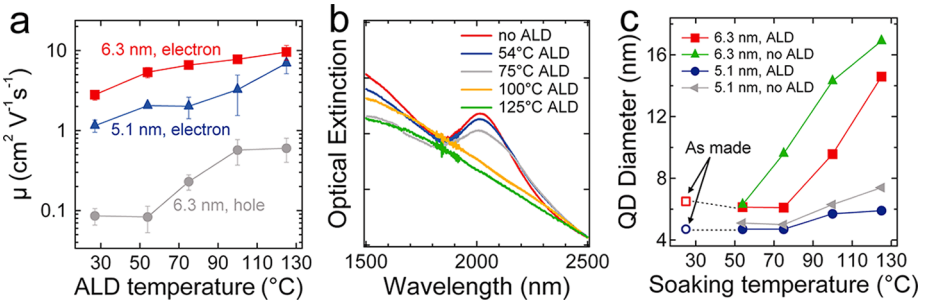

Figure 5. (a) Linear field-effect mobility of alumina-infilled, sulfide-treated QD FETs as a function of ALD growth temperature. Squares = electron mobility of 6.3 nm QDs; circles = hole mobility of 6.3 nm QDs; triangles = electron mobility of 5.1 nm QDs. The smaller QDs show only *n*-channel transport (no hole data). Each data point is the average of 6−10 devices prepared over the course of several months. QD film thickness = 20−35 nm; ALD alumina thickness =18−25 nm. Channel dimensions: length = 25 μm; width = 1000 μm. V_{SD} = ±10 V (<3 mV voltage drop per QD). (b) Optical extinction spectra of 6.3 nm QD films before ALD infilling and after infilling at 54, 75, 100, and 125 °C. The exciton peak is washed out after infilling at ≥100 °C. Spectra are aligned at 2500 nm. Note that the weak scattering tail extending past 2500 nm is not shown in these spectra. Film thickness: ~150 nm. Alumina thickness: 18−25 nm. (c) Average QD diameter versus ALD growth or annealing temperature as computed from Scherrer fits of {111} XRD peaks from each film. Data are shown for both QD sizes. Data labeled "ALD" are 9 h ALD runs at the indicated temperatures. Alumina thickness: 15−25 nm. Data labeled "no ALD" are control experiments in which films were exposed to the growth conditions in the ALD chamber (temperature and pressure) for 9 h but without alumina deposition. Heating without ALD results in a larger increase in grain size because no ALD matrix is present to retard diffusion within the films.

conductance with quasi-linear *I*−*V*s and high off currents, consistent with a large concentration of holes in the film that cannot easily be modulated by the applied gate field. The linear hole mobility (V_{SD} = −10 V) calculated from eq 1 for a series of identical FETs is 0.1−0.15 cm^2 V^{-1} s^{-1}, which is 3−5 times larger than the hole mobility of EDT-treated FETs using the same QD size.[18] The larger hole mobility of sulfide-treated FETs may be due to the smaller interdot distance and better electronic coupling afforded by the smaller sulfide ligand ($d_{S^{2-}}$ ≈ 3.5 Å, $d_{EDT^{2-}}$ ≈ 8 Å; see Figure 2).[40] After ALD infilling and overcoating, the FET becomes ambipolar with a dominant n-channel and weak p-channel, decent on−off ratios (>1000), and nearly ideal *I*−*V* curves (Figure 4c,d). The electron and hole mobility for a series of FETs infilled at 54 °C is 4.5−6.1 and 0.07−0.2 cm^2 V^{-1} s^{-1}, respectively (V_{SD} = ±10 V).

Both the electron and hole mobilities increase with the ALD infilling temperature (Figure 5a). The average electron mobility for 6.3 nm QD films increases from 2.8 cm^2 V^{-1} s^{-1} at 27 °C to 9.6 cm^2 V^{-1} s^{-1} at 125 °C, while the average hole mobility increases from 0.086 to 0.6 cm^2 V^{-1} s^{-1} over the same ALD temperature range. A similar trend is also observed for electron transport in smaller QDs (5.1 nm), but with somewhat lower mobilities.[18] Since PbX QDs can neck, ripen, and sinter at surprisingly low temperatures,[27,41] we measured the average size and size distribution of the QDs in each film using optical extinction spectroscopy and X-ray diffraction (XRD). Optical spectra show that the first exciton peak of 6.3 nm QD films washes out when the ALD temperature is ≥100 °C because Ostwald ripening causes a large increase in the distribution of QD sizes and optical band gaps (Figure 5b). XRD peak fitting with the Scherrer size broadening equation indicates that the average QD size remains unchanged for ALD infilling temperatures as high as 75 °C (red data in Figure 5c). The average grain size then increases to 9.6 nm at 100 °C and 14.6 nm at 125 °C. This increase in average size indicates that the 6.3 nm PbSe QDs extensively neck and sinter when the ALD temperature is above ~75 °C. We recently studied similar phenomena in PbS QD films.[27] Therefore, we attribute the increase in carrier mobility above 75 °C primarily to QD sintering that reduces the number of interdot barriers to charge transport. A similar but subtler trend is observed for 5.1 nm QDs (blue data in Figure 5c). To avoid such sintering effects, we focus hereafter only on low-temperature ALD (≤75 °C) in order to produce high-mobility QD FETs in which the QDs retain their original identity, including their physical size, shape, and band gap. FETs infilled at the maximum safe temperature (75 °C) show a linear electron mobility of 6−8 cm^2 V^{-1} s^{-1}, equal to the highest mobility values yet reported for PbX QD FETs. Moreover, these high-mobility FETs are stable indefinitely in air (Figure 6) because, as we recently

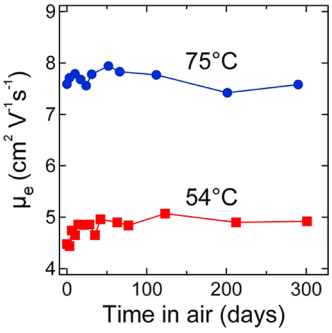

Figure 6. Electron mobility of PbSe QD FETs infilled at 54 and 75 °C as a function of time stored in air. Films were stored in the dark and at room temperature. QD diameter: 6.3 nm. ALD alumina thickness: 25 nm.

demonstrated, the ALD infill and overcoat form an extremely effective gas diffusion barrier that stops oxidation and inhibits internal diffusion within the films.[28] These sulfide-treated, ALD-infilled PbSe QD FETs are the first high-mobility, air stable PbX QD solids and should be useful in the development of high-performance QD optoelectronic devices.

We performed a series of control experiments to determine if the observed changes in carrier type and mobility result from infilling of the QD film or from some other factor, such as modification of the gate oxide by alumina, film heating, film annealing, or measurement artifacts. We first tested if changes to the gate oxide were responsible for the observed behavior, but sulfide-capped QD films deposited on the normal SiO_2 gate oxide and on this oxide coated with 2−3 nm of alumina had

dx.doi.org/10.1021/nl304753n | Nano Lett. 2013, 13, 1578−1587

very similar $I-V$ curves (Supporting Information Figure S3), clearly demonstrating that modification of the gate dielectric by ALD does not cause the changes in FET characteristics. Next we considered the impact of film heating. Extended heating without ALD yielded a modest increase in hole mobility but no other significant changes to the $I-V$ curves (Supporting Information Figure S4). We can therefore rule out film heating per se (e.g., QD necking, settling, and densification of the films, etc.). We further found that soaking partially-infilled FETs at the ALD growth temperature for long times did not cause additional changes to the $I-V$ characteristics; that is, the FETs evolve with more ALD cycles (see below), but not with more time at elevated temperatures.

We also assessed whether the FET changes could be an artifact caused by different drain current (I_D) transients[17,18,42,43] before and after ALD infilling. Supporting Information Figures S5 and S6 compare I_D transients for typical FETs before and after ALD infilling (75 °C) at room temperature (300 K) and low temperature (80 K). At room temperature, sulfide-capped PbSe QD films without ALD show dramatic I_D transients, but the transients become much less pronounced after ALD infilling. For FETs without ALD, stepping the gate voltage causes a sudden change in I_D, as expected, but this is followed by an anomalous stretched exponential decay of I_D (that is, a transient, also called bias-stress effect). We previously attributed such I_D transients to screening of the applied gate field, possibly by charge trapped on the first layer of QDs.[17,18] Others have since observed similar I_D transients in PbX QD FETs.[42,43] The transients are suppressed by ALD perhaps because the alumina coating passivates many of the surface traps responsible for gate screening; alternatively, the ALD matrix may inhibit whatever ligand or QD motion causes the transients.[43,44] The transients are also thermally activated (Supporting Information Figures S5 and S6). Activated I_D transients in PbX QD FETs have been observed by others and attributed to a barrier to trapping,[42] thermally activated ligand rearrangements,[43] or QD motion. Below ~150 K, the transients were greatly suppressed for FETs without ALD and often completely eliminated for infilled FETs. Crucially, however, elimination of the transients at low temperature did not result in changes in dominant carrier type or mobility: FETs without ALD remained p-channel devices with no sign of n-channel conductivity, while infilled FETs remained high-mobility n-channel devices at all temperatures (Supporting Information Figures S5 and S6). These experiments show that suppression of the transients as a result of ALD infilling causes neither the change in carrier type nor the high electron mobility observed in these devices.

As a final check, we examined the dependence of the carrier mobility on the V_G sweep rate to test the possibility that the high electron mobility of infilled FETs is an artifact of fast V_G scanning. Figure 7 shows the electron and hole mobility versus sweep rate at 300 and 80 K for a typical device infilled at 75 °C. The electron mobility is independent of sweep rate from 0.01 to 50 V/s. The hole mobility increases by about a factor of 4 over the same range of sweep rate, which is caused by persistent I_D transients for holes, even at low temperatures.[42,43] Together, these control experiments firmly establish that the change in dominant carrier type and mobility is a consequence of alumina infilling of the sulfide-capped QD films; that is, it is a property of the $PbSe/Al_2O_3$ nanocomposite film itself, rather than a result of modifications to the gate dielectric, film heating, film annealing, or artifacts stemming from time-dependent drain currents.

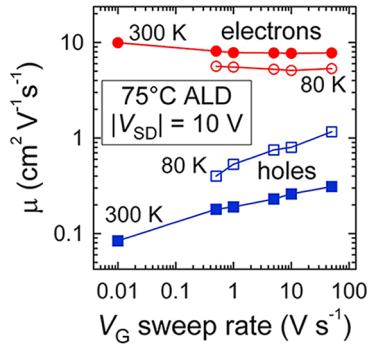

Figure 7. Effect of V_G sweep rate on the mobility measured for a typical QD FET infilled at 75 °C. Data at both 300 K (closed symbols) and 80 K (open symbols) are shown. The electron mobility is essentially independent of sweep rate, while the hole mobility decreases by a factor of ~4 due to a persistent I_D transient for holes. $V_{SD} = \pm 10$ V. Note that the electron mobility slightly decreases and the hole mobility increases at lower temperatures. See Supporting Information Figure S7 for a plot of mobility versus temperature for typical devices.

Having confirmed that alumina infilling causes the observed FET behavior, we now explain how it does so. Figure 8 shows that the transfer characteristics and carrier mobilities evolve systematically with the number of ALD cycles for the first ~40

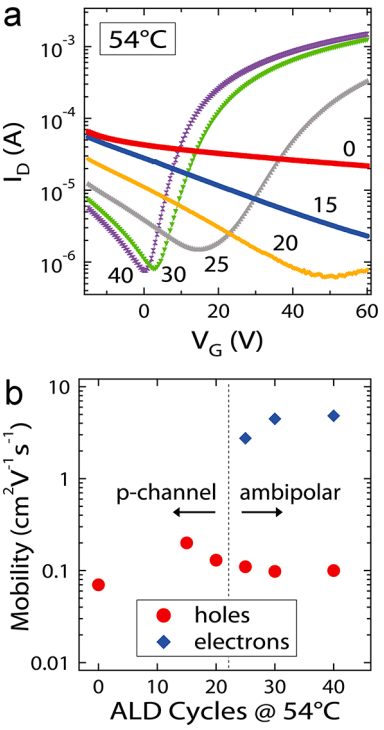

Figure 8. Evolution of FET behavior with the number of ALD cycles. (a) Transfer curves of six devices measured at $V_{SD} = +10$ V at room temperature, showing a systematic change from p-channel transport to n-channel dominated ambipolar transport from 0 to 40 ALD cycles. The transfer curves stop changing after ~40 ALD cycles, corresponding to an effective alumina thickness of ~5 nm. (b) Linear mobility values for these six devices. The hole mobility initially increases by a factor of 2–3 and then settles to ~0.1 $cm^2\ V^{-1}\ s^{-1}$. A measurable n-channel appears only after >20 ALD cycles. The electron mobility increases and then plateaus at ~4.8 $cm^2\ V^{-1}\ s^{-1}$. QD diameter: 6.3 nm. ALD temperature: 54 °C. Sweep rates = 50 V/s.

dx.doi.org/10.1021/nl304753n | Nano Lett. 2013, 13, 1578–1587

cycles. The films, which initially act as p-channel depletion mode FETs with poor gate modulation, steadily become ambipolar after 20−25 ALD cycles and then n-channel-dominated enhancement mode FETs with good gate modulation after 30−40 ALD cycles. The hole current decreases, electron current increases, and threshold voltage shifts from a large positive value to ∼0 V. Deposition of more than ∼40 cycles of ALD results in no further change to the transfer curves because the films are totally infilled at this point and additional ALD only adds to the thickness of the overcoat, which is electrically inactive. We believe that these changes in FET behavior result from the passivation of acceptor states and electron traps on the QD surfaces by the growing alumina layer. As a starting point, we assume that sulfide ions adsorbed on PbSe QDs act as acceptor dopants and cause the moderately high hole concentration in sulfide-treated films prior to ALD infilling. Unpassivated chalcogenide ions on the surface of nonstoichiometric CdX and PbX QDs are believed to be acceptors.[45−48] The high hole concentration explains why the FETs show high p-channel conductance with weak gate modulation and a low on/off ratio (the large doping prevents these devices from being turned off by the gate). It is also the reason that sulfide-treated films on glass substrates are p-type in thermopower measurements (see Methods). Infilling with ALD alumina has two major effects on the electronic properties of these films. First, alumina deposition steadily passivates the acceptors and lowers the hole concentration, causing the FETs to evolve from unipolar p-channel transport before ALD to ambipolar transport after 20−25 ALD cycles and then to dominant n-channel transport for >30 ALD cycles. This decrease in hole concentration is responsible for the negative shift in threshold voltage to ∼0 V and the switch in dominant carrier type from holes to electrons seen in Figure 8. Thermopower measurements confirmed that films on glass become n-type after ALD infilling. XPS measurements verified that alumina is indeed deposited in the films starting from the first several ALD cycles (see Supporting Information Figures S8−S10).

The second effect of alumina infilling is to increase the electron mobility by passivating electron surface traps within the QD band gap. Trap passivation can explain the observed increase in electron mobility with both the number of ALD cycles (a more complete alumina coating gives better passivation, Figure 8b) and the ALD temperature (higher temperature increases precursor reactivity and gives more complete surface reactions, Figure 5a). Evidence for trap passivation comes from comparing the dependence of mobility on gate bias for devices before and after ALD infilling (Figure 9). Accurate measurements of μ_{lin} as a function of V_G require FETs with ideal $I-V$ characteristics at small V_{SD}. We used a gated 4-point FET geometry featuring gold electrodes with especially thin titanium adhesions layers (∼1 nm) to eliminate contact resistance and the slightly nonlinear $I-V$ characteristics of our normal devices at small V_{SD} (see Figure 4b and Supporting Information Figure S2 for examples of these nonlinear $I-V$s, which we believe are caused by an injection barrier between the QDs and titanium). The measurements were performed at 80 K to quench the I_D transient and simplify comparisons between devices before and after ALD (see above). As shown in Figure 9, FETs without ALD have a hole mobility that increases dramatically with $|V_G|$ and then levels off at $V_G < -40$ V. Such gate-dependent mobility is common for disordered semiconductors such as amorphous silicon,[49]

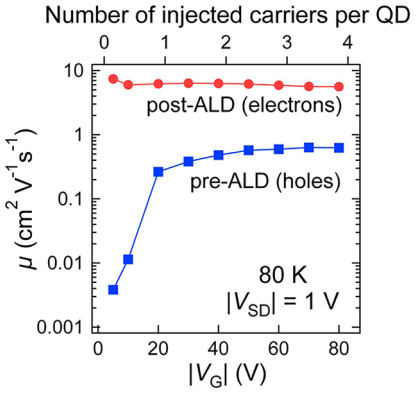

Figure 9. Carrier mobility versus the absolute value of V_G for sulfide-capped PbSe QD FETs before and after full ALD infilling at 75 °C. The devices were measured at 80 K and $|V_{SD}| = 1$ V using a gated 4-point FET geometry to eliminate contact resistance and other distortions. Note that the carrier density (top axis) is an upper limit and may be overestimated by as much as a factor of 3 (see Methods). See Supporting Information Figure S11 for plots of mobility versus V_{SD} for these devices.

organics,[50] and nanocrystalline TiO_2[51] in which carrier mobility increases with carrier density as a result of trap filling.[52,53] The average hole density induced in the accumulation layer by the gate bias is $p = C_{ox}(V_G - V_D/2 - V_T)/e$, corresponding to ∼1.9 holes per QD at the bias where the mobility saturates ($V_G \sim -40$ V). At this large V_G, the Fermi level is close to the $1S_h$ level, most of the traps are filled (including deep gap states and band tail states), and the activation energy for detrapping is minimized, so the mobility is maximized. Above this gate bias, injected carriers move primarily through the $1S_h$ QD states with a mobility limited by the interdot electronic coupling, confinement disorder, and QD charging energy rather than the density of states in the QD band gap. In contrast to the highly gate-dependent mobility of FETs without ALD, FETs with ALD show a high (electron) mobility that does not increase with V_G because the trap density in these films is low as a result of ALD infilling. With few traps to contend with, carriers injected into the infilled films can readily access the $1S_e$ QD states even at small values of V_G, giving a mobility that is nearly independent of gate bias. A close look at Figure 9 reveals that the electron mobility actually decreases somewhat with V_G, possibly because of enhanced electron−electron interactions at higher carrier densities. Overall, our mobility versus V_G data show that ALD infilling greatly reduces the concentration of localized gap states in sulfide-capped PbSe QD FETs. We conclude that trap passivation by the alumina coating is the main cause of the high electron mobility in these devices.

Alternative explanations for the impact of the ALD alumina coating, for example, that it lowers the tunnel barrier height or reduces the QD charging energy, are unable to account for the main observations, including the polarity switch and the increase in electron mobility with ALD temperature. We rule out tunnel barrier lowering because alumina is a very wide bandgap insulator ($E_g > 7$ eV). Moreover, although the QD charging energy certainly decreases when interstitial voids ($\varepsilon \sim 1$) are infilled with amorphous alumina ($\varepsilon \sim 8-11$),[54] the charging energy of a 6 nm PbSe QD in a random close-packed QD film is already less than 10−15 meV,[18] making the impact of any further decrease in charging energy relatively unimportant for room-temperature transport.

dx.doi.org/10.1021/nl304753n | Nano Lett. 2013, 13, 1578−1587

We note that that the electron mobility of sulfide-capped films may be fairly high (~1 cm^2 V^{-1} s^{-1}) even before ALD infilling and merely impossible to observe in FET *I*–*V*s due to the overwhelming concentration of majority holes. If this is the case, then the first 20–25 ALD cycles lowers the hole concentration enough to reveal preexisting high-mobility electron transport. Trap passivation by the ALD coating would then be responsible for increasing the mobility above 1 cm^2 V^{-1} s^{-1}. Looking to the future, it should be possible to prepare optimized p-type QD films for solar cells by using ALD to tune the concentration of majority holes and thus the film conductivity while maintaining a high mobility for minority electrons. Since the high electron mobility is achieved partly by passivating surface defects, the mobility-lifetime product should be especially large in these films. We are currently exploring the use of such strategies to boost the minority carrier diffusion length, photocurrent, and power conversion efficiency of QD solar cells.

It is important to consider whether QD FET mobilities are relevant to QD solar cells. There are several important differences between a field-effect mobility and the field-free mobility of carriers in a QD film used as the active layer in a solar cell. First, charge transport in FETs is effectively two-dimensional with over 90% of the induced charge concentrated in the first 10 nm or so of the QD film under most bias conditions (see the discussion of the accumulation layer thickness in the Supporting Information), while mobility in a QD film is fully three-dimensional. Second, unipolar FETs provide information on the majority carrier mobility, but the minority carrier mobility is the important parameter in most solar cells. Ambipolar FETs, such as the ALD-infilled devices studied here, avoid this limitation by enabling the measurement of both types of carriers in the same device. Third, FET mobilities are measured under high injected carrier density, trap-filled conditions and, as a result, are in general much larger than mobilities in QD films at equilibrium carrier density. Even the mechanism of charge transport may be different in QD FETs and solar cells because of different Fermi level positions and gap state occupancy. Since FET mobilities may grossly overestimate the actual field-free mobility in a QD solar cell, FET data must be applied to solar cells with caution. In the case of QD FETs that have few gap states and weak dependence of mobility on gate bias, the FET mobility and field-free mobility should be comparable and the FET mobility can be used to describe solar cells based on similarly-prepared QD films. This is the situation for our sulfide-capped, ALD-infilled devices. When QD FETs have a large concentration of gap states and strong dependence of mobility on gate bias, the question is whether solar illumination can mimic the effect of the gate bias by filling traps to give an "illuminated mobility" that is similar in magnitude to the dark field-effect mobility. For example, the carrier mobility in nanocrystalline TiO_2 films increases by orders of magnitude upon ~1 sun illumination as a result of trap filling.[51,53] A similar effect should occur in illuminated PbX QD films. The density of photogenerated charges (n) can be estimated from the product of the generation rate (G) and the carrier lifetime (τ), $n = G\tau$. While G is small because of the low flux of solar photons (4×10^{17} photons cm^{-2} s^{-1} for the standard AM 1.5G spectrum), τ may be quite large depending on the density, cross section, and energy distribution of traps in the QD film, so n can approach the charge density achieved in FETs at large gate bias. If trap filling is indeed significant at solar light intensities, then QD FET mobilities should apply in a semiquantitative way to illuminated QD solar cells, making ambipolar FETs a useful platform for optimizing charge transport in QD films for solar cells.

■ ASSOCIATED CONTENT

Ⓢ Supporting Information

Figures S1–S13, discussion of accumulation layer thickness. This material is available free of charge via the Internet at http://pubs.acs.org.

■ AUTHOR INFORMATION

Corresponding Author

*E-mail: matt.law@uci.edu.

Author Contributions

⊥These authors contributed equally to this work.

Notes

The authors declare no competing financial interest.

■ ACKNOWLEDGMENTS

Y.L., M.G., Y.L., and J.C.H. are supported by the Center for Advanced Solar Photophysics (CASP), an Energy Frontier Research Center funded by the U.S. Department of Energy (DOE), Office of Science, Office of Basic Energy Sciences (BES). R.I. and M.L. are supported by the Department of Energy under Award DE-SC0003904. J.T. acknowledges support from an NSF Graduate Research Fellowship. Work at NREL was funded by the U.S. Department of Energy under Contract No. DE-AC36-G028308. We thank the UCI School of Physical Sciences Center for Solar Energy.

■ REFERENCES

(1) Kovalenko, M. V.; Scheele, M.; Talapin, D. V. *Science* **2009**, *324*, 1417–1420.

(2) Talapin, D. V.; Lee, J.-S.; Kovalenko, M. V.; Shevchenko, E. V. *Chem. Rev.* **2010**, *110*, 389–458.

(3) Nozik, A. J.; Beard, M. C.; Luther, J. M.; Law, M.; Ellingson, R. J.; Johnson, J. C. *Chem. Rev.* **2010**, *110*, 6873–6890.

(4) Hanrath, T. *J. Vac. Sci. Technol., A* **2012**, *30*, 030802.

(5) Kovalenko, M. V.; Bodnarchuk, M. I.; Zaumseil, J.; Lee, J.-S.; Talapin, D. V. *J. Am. Chem. Soc.* **2010**, *132*, 10085–10092.

(6) Lee, J.-S.; Kovalenko, M. V.; Huang, J.; Chung, D. S.; Talapin, D. V. *Nat. Nanotechnol.* **2011**, *6*, 348–352.

(7) Chung, D. S.; Lee, J.-S.; Huang, J.; Nag, A.; Ithurria, S.; Talapin, D. V. *Nano Lett.* **2012**, *12*, 1813–1820.

(8) Kovalenko, M. V.; Schaller, R. D.; Jarzab, D.; Loi, M. A.; Talapin, D. V. *J. Am. Chem. Soc.* **2012**, *134*, 2457–2460.

(9) Nag, A.; Kovalenko, M. V.; Lee, J.-S.; Liu, W.; Spokoyny, B.; Talapin, D. V. *J. Am. Chem. Soc.* **2011**, *133*, 10612–10620.

(10) Zhang, H.; Hu, B.; Sun, L.; Hovden, R.; Wise, F. W.; Muller, D. A.; Robinson, R. D. *Nano Lett.* **2011**, *11*, 5356–5361.

(11) Tang, J.; Kemp, K. W.; Hoogland, S.; Jeong, K. S.; Liu, H.; Levina, L.; Furukawa, M.; Wang, X.; Debnath, R.; Cha, D.; Chou, K. W.; Fischer, A.; Amassian, A.; Asbury, J. B.; Sargent, E. H. *Nat. Mater.* **2011**, *10*, 765–771.

(12) Fafarman, A. T.; Koh, W.; Diroll, B. T.; Kim, D. K.; Ko, D.-K.; Oh, S. J.; Ye, X.; Nguyen, V. D.; Crump, M. R.; Reifsnyder, D. C.; Murray, C. B.; Kagan, C. R. *J. Am. Chem. Soc.* **2011**, *133*, 15753–15761.

(13) Koh, W.; Saudari, S. R.; Fafarman, A. T.; Kagan, C. R.; Murray, C. B. *Nano Lett.* **2011**, *11*, 4764–4767.

(14) Choi, J.-H.; Fafarman, A. T.; Oh, S. J.; Ko, D.-K.; Kim, D. K.; Diroll, B. T.; Muramoto, S.; Gillen, J. G.; Murray, C. B.; Kagan, C. R. *Nano Lett.* **2012**, *12*, 1631–2638.

(15) Rosen, E. L.; Buonsanti, R.; Llordes, A.; Sawvel, A. M.; Milliron, D. J.; Helms, B. A. *Angew. Chem., Int. Ed.* **2012**, *51*, 684–689.

(16) Talapin, D. V.; Murray, C. B. *Science* **2005**, *310*, 86−89.
(17) Luther, J. M.; Law, M.; Song, Q.; Beard, M. C.; Nozik, A. J. *ACS Nano* **2008**, *2*, 271−280.
(18) Liu, Y.; Gibbs, M.; Puthussery, J.; Gaik, S.; Ihly, R.; Hillhouse, H. W.; Law, M. *Nano Lett.* **2010**, *10*, 1960−1969.
(19) Guyot-Sionnest, P. *J. Phys. Chem Lett.* **2012**, *3*, 1169−1175.
(20) Oh, S. J.; Berry, N. E.; Choi, J.-H.; Gaulding, E. A.; Paik, T.; Hong, S.-H.; Murray, C. B.; Kagan, C. R. *ACS Nano*, Article ASAP; DOI: 10.1021/nn3057356.
(21) Nagpal, P.; Klimov, V. I. *Nat. Commun.* **2011**, *2*, 486.
(22) Ip, A. H.; Thon, S. M.; Hoogland, S.; Voznyy, O.; Zhitomirsky, D.; Debnath, R.; Levina, L.; Rollny, L. R.; Carey, G. H.; Fischer, A.; Kemp, K. W.; Kramer, I. J.; Ning, Z.; Labelle, A. J.; Chou, K. W.; Amassian, A.; Sargent, E. H. *Nat. Nanotechnol.* **2012**, *7*, 577−582.
(23) Gao, J.; Johnson, J. C. *ACS Nano* **2012**, *6*, 3292−3303.
(24) Erslev, P. T.; Chen, H.-Y.; Gao, J.; Beard, M. C.; Frank, A. J.; van de Lagemaat, J.; Johnson, J. C.; Luther, J. M. *Phys. Rev. B* **2012**, *86*, 155313.
(25) Kang, M. S.; Lee, J.; Norris, D. J.; Frisbie, C. D. *Nano Lett.* **2009**, *9*, 3848−3852.
(26) Xia, Y.; Cho, J. H.; Lee, J.; Ruden, P. P.; Frisbie, C. D. *Adv. Mater.* **2009**, *21*, 2174.
(27) Ihly, R.; Tolentino, J.; Liu, Y.; Gibbs, M.; Law, M. *ACS Nano* **2011**, *5*, 8175−8186.
(28) Liu, Y.; Gibbs, M.; Perkins, C. L.; Tolentino, J.; Zarghami, M. H.; Bustamante, J., Jr.; Law, M. *Nano Lett.* **2011**, *11*, 5349−5355.
(29) Kinder, E.; Moroz, P.; Diederich, G.; Johnson, A.; Kirsanova, M.; Nemchinov, A.; O'Conner, T.; Roth, D.; Zamkov, M. *J. Am. Chem. Soc.* **2011**, *133*, 20488−20499.
(30) George, S. M. *Chem. Rev.* **2010**, *110*, 111−131.
(31) Kim, H. *J. Vac. Sci. Technol., B* **2003**, *21*, 2231−2261.
(32) Law, M.; Beard, M. C.; Choi, S.; Luther, J. M.; Hanna, M. C.; Nozik, A. J. *Nano Lett.* **2008**, *8*, 3904−3910.
(33) Perdew, J. P.; Burke, K.; Ernzerhof, M. *Phys. Rev. Lett.* **1996**, *77*, 3865−3868.
(34) Weigend, F.; Ahlrichs, R. *Phys. Chem. Chem. Phys.* **2005**, *7*, 3297.
(35) TURBOMOLE V6.4 2012, a development of University of Karlsruhe and Forschungszentrum Karlsruhe GmbH, 1989−2007, TURBOMOLE GmbH, since 2007; available from www.turbomole.com.
(36) Nag, A.; Kovalenko, M. V.; Lee, J.-S.; Liu, W.; Spokoyny, B.; Talapin, D. V. *J. Am. Chem. Soc.* **2011**, *133*, 10612.
(37) Moreels, I.; Fritzinger, B.; Martins, J. C.; Hens, Z. *J. Am. Chem. Soc.* **2008**, *130*, 15081−15086.
(38) Bealing, C. R.; Baumgardner, W. J.; Choi, J. J.; Hanrath, T.; Hennig, R. G. *ACS Nano* **2012**, *6*, 2118−2127.
(39) Moreels, I.; Lambert, K.; Muynck, D. D.; Vanhaecke, F.; Poelman, D.; Martins, J. C.; Allan, G.; Hens, Z. *Chem. Mater.* **2007**, *19*, 6101−6106.
(40) The diameter of S^{2-} is taken to be twice its ionic radius (1.8 Å). The length of EDT^{2-} (ethanedithiolate, doubly deprotonated EDT) is determined as the sum of the S-to-S internuclear distance of EDT (4.35 Å according to the hybrid density functional PBE0 and basis set def2-TZVP) and two sulfur radii (1.8 Å). Note that the interdot distance can be smaller than the length of EDT^{2-} if the adsorbed ligands are not perpendicular to the QD surface (as in Figure 2).
(41) van Huis, M. A.; Kunneman, L. T.; Overgaag, K.; Xu, Q.; Pandraud, G.; Zandbergen, H. W.; Vanmaekelbergh, D. *Nano Lett.* **2008**, *8*, 3959−3963.
(42) Kang, M. S.; Sahu, A.; Norris, D. J.; Frisbie, C. D. *Nano Lett.* **2011**, *11*, 3887−3892.
(43) Osedach, T. P.; Zhao, N.; Andrew, T. L.; Brown, P. R.; Wanger, D. D.; Strasfeld, D. B.; Chang, L.-Y.; Bawendi, M. G.; Bulovic, V. *ACS Nano* **2012**, *6*, 3121−3127.
(44) Nelson, C. A.; Zhu, X. Y. *J. Am. Chem. Soc.* **2012**, *134*, 7592−7595.
(45) Gomez-Campos, F. M.; Califano, M. *Nano Lett.* **2012**, *12*, 4508−4517.
(46) Franceschetti, A. *Phys. Rev. B* **2008**, *78*, 075418.
(47) Bryant, G. W.; Jaskolski, W. *J. Phys. Chem. B* **2005**, *109*, 19650−19656.
(48) Gai, Y.; Peng, H.; Li, J. *J. Phys. Chem. C* **2009**, *113*, 21506−21511.
(49) Shur, M.; Hack, M.; Shaw, J. G. *J. Appl. Phys.* **1989**, *66*, 3371−3380.
(50) Pesavento, P. V.; Puntambekar, K. P.; Frisbie, C. D.; McKeen, J. C.; Ruden, P. P. *J. Appl. Phys.* **2006**, *99*, 094504.
(51) Fisher, A. C.; Peter, L. M.; Ponomarev, E. A.; Walker, A. B.; Wijayantha, K. G. U. *J. Phys. Chem. B* **2000**, *104*, 949−958.
(52) Horowitz, G. *Adv. Mater.* **1998**, *10*, 365−377.
(53) Dimitrakopoulos, C. D.; Purushothaman, S.; Kymissis, J.; Callegari, A.; Shaw, J. M. *Science* **1999**, *283*, 822−824.
(54) Momida, H.; Hamada, T.; Takagi, Y. *Phys. Rev. B* **2006**, *73*, 054108.
(55) Kopidakis, N.; Sciff, E. A.; Park, N.-G.; van de Lagemaat, J.; Frank, A. J. *J. Phys. Chem. B* **2000**, *104*, 3930−3936.